



Original Research *Neuroradiology/Head and Neck Imaging*

Optimization of image quality and diagnostic accuracy for vascular stenosis in computed tomography perfusion-reconstructed cerebral computed tomography angiography using deep learning reconstruction

Lulu Zhang^{1#}, Xianghao Feng^{1#}, He Zhang², Dapeng Zhang², Houliang Zhao², Qihang Sun³, Yankai Meng², Cunjie Sun²

¹School of Medical Technology, Xuzhou Medical University, ²Department of Radiology, Affiliated Hospital of Xuzhou Medical University, Xuzhou, Jiangsu, China, ³School of Medicine and Health, Technical University of Munich, Munich, Germany.

#These author contributed equally to this work.



***Corresponding author:**

Cunjie Sun,
Department of Radiology,
Affiliated Hospital of Xuzhou
Medical University, Xuzhou,
Jiangsu, China.

suncunjie@126.com

Received: 09 September 2025

Accepted: 20 November 2025

Published: 17 March 2026

DOI

10.25259/JCIS_226_2025

Quick Response Code:



ABSTRACT

Objectives: This study aims to compare the effects of deep learning image reconstruction (DLIR) and adaptive statistical iterative reconstruction-veo (ASIR-V) algorithms on the image quality of cranial computed tomography angiography (CTA) reconstructed from computed tomography perfusion (CTP) data and to evaluate their agreement with digital subtraction angiography (DSA), the gold standard for diagnosing arterial stenosis.

Material and Methods: This retrospective study enrolled patients with clinically suspected cerebrovascular disease who had undergone CTP examination. From the arterial peak phase of CTP raw data, four CTA datasets were reconstructed: ASIR-V 40%, ASIR-V 80%, DLIR low setting (DLIR-L), and DLIR high setting (DLIR-H). Regions of interest were placed at the M1 segment of the middle cerebral artery (MCA), basilar artery (BA), and internal carotid artery (ICA) on the healthy side and the temporalis muscle. Computed tomography attenuation values and standard deviations were measured, and the contrast-to-noise ratio (CNR) and signal-to-noise ratio (SNR) were subsequently calculated using the attenuation values and standard deviations. Vessel edge sharpness was objectively assessed using edge rise distance (ERD) and edge rise slope (ERS). Using DSA as the reference standard, diagnostic performance for vascular stenosis was evaluated, and agreement was analyzed with the Kappa test. Two radiologists independently scored subjective image quality using a 5-point Likert scale.

Results: Sixty-five patients were included, 14 of whom additionally underwent DSA. For the MCA, ICA, and BA, image noise in the DLIR-H group was significantly lower than that in the other groups, with statistically significant differences compared with ASIR-V 40% ($p < 0.05$). For CNR and SNR, DLIR-H and ASIR-V 80% outperformed ASIR-V 40% and DLIR-L across all arterial levels ($p < 0.05$). ERD and ERS were significantly superior in the DLIR groups compared with the ASIR-V groups ($p < 0.05$). In subjective evaluations, the DLIR-H group achieved the highest scores across all parameters ($p < 0.05$). Agreement with DSA was excellent for DLIR-H ($\kappa = 0.819$), significantly higher than for ASIR-V ($p < 0.05$).

Conclusion: In CTP examinations for suspected cerebrovascular disease, DLIR-H markedly improves cranial CTA image quality compared with ASIR-V, while achieving higher diagnostic agreement with DSA. DLIR-H can be recommended as the preferred clinical reconstruction method.

Keywords: Adaptive statistical iterative reconstruction-Veo, Computed tomography angiography, Computed tomography perfusion, Deep learning reconstruction algorithm, Digital subtraction angiography

This is an open-access article distributed under the terms of the Creative Commons Attribution-Non Commercial-Share Alike 4.0 License, which allows others to remix, transform, and build upon the work non-commercially, as long as the author is credited and the new creations are licensed under the identical terms.

©2026 Published by Scientific Scholar on behalf of Journal of Clinical Imaging Science

INTRODUCTION

Stroke is a common cerebrovascular disease characterized by high incidence, mortality, disability, and recurrence rates.^[1] In recent years, it has exhibited a trend toward a younger onset.^[2] Early diagnosis and evaluation are therefore crucial for effective treatment and improved prognosis.^[3] Digital subtraction angiography (DSA) is considered the gold standard for vascular diagnosis and assessment owing to its high spatial resolution and real-time dynamic imaging capabilities.^[4] However, due to its risks, including high ionizing radiation exposure and the nephrotoxic effects of iodine-based contrast agents, DSA is generally not recommended as the first-choice imaging modality for patients with stroke.^[5]

Cerebral computed tomography perfusion (CTP) enables quantitative assessment of cerebral hemodynamics and accurate detection of abnormal cerebral blood perfusion in stroke patients.^[6,7] It can provide whole-brain perfusion maps and generate 4D computed tomography angiography (CTA) images. These images can replace traditional CTA for evaluating vasospasm while reflecting intracranial collateral circulation and vascular conditions.^[8-10] However, CTP requires continuous repeated scanning of the target area during contrast agent injection,^[6] which increases patients' radiation exposure risk. Therefore, reducing radiation dose concerns is essential to ensure both patient safety and diagnostic effectiveness.

Beyond the effects of tube voltage, tube current, and scan frequency, previous studies have demonstrated that image reconstruction algorithms also significantly influence both radiation dose and image quality.^[11,12] With the rapid development of computer technology, iterative reconstruction (IR) algorithms have emerged as the mainstream reconstruction approach in computed tomography (CT) imaging. Adaptive statistical IR-Veo (ASIR-V; GE Healthcare, USA) is a vendor-specific hybrid IR technology. Compared with other IR methods, ASIR-V can reduce image noise and radiation dose while achieving shorter reconstruction times.^[13] However, similar to other IR techniques, the ASIR-V algorithm faces limitations, particularly the difficulty of balancing image noise reduction with maintaining natural image texture.^[14]

With the rapid advancement of artificial intelligence, deep learning technology has been widely applied to CT image reconstruction. Deep learning image reconstruction (DLIR) algorithms have been demonstrated to reduce noise and enhance diagnostic accuracy under low-dose conditions.^[15] By training on large-scale, high-quality conventional-dose CT images and their corresponding low-dose images or raw original projection data, DLIR algorithms learn to distinguish between true signals and noise, capturing both

local detail and global image structure.^[16] This technology has been applied in various clinical settings, including pediatric "dual-low" chest CTA and abdominal dual-energy CT.^[17,18] By modeling the natural noise distribution of normal tissues, DLIR can substantially reduce radiation dose while preserving the authenticity of noise texture, maintaining high spatial resolution, and clearly depicting critical anatomical details such as fine structures and small vessel branches,^[19] thereby producing higher-quality images. However, the clinical value of DLIR for improving cranial CTA image quality based on CTP data has not been fully explored.

Therefore, this study was performed to evaluate the image quality of CTA using DLIR in CTP compared with the ASIR-V algorithm. In addition, it assessed the diagnostic performance of these reconstruction methods against DSA in detecting arterial stenosis.

MATERIAL AND METHODS

The Medical Ethics Committee of the Affiliated Hospital of Xuzhou Medical University approved this study (XYFY2025-KL284-01). In total, 65 patients who underwent CTP examinations at our hospital between June 2024 and June 2025 were retrospectively enrolled. Of these, 14 patients underwent both CTP and DSA examinations [Figure 1].

Inclusion criteria

The inclusion criteria were an age of ≥ 18 years; clinically suspected acute cerebral infarction, with cerebral CT plain scan and CTP examination performed within 24 h of symptom onset; and no prior history of large-area ischemic stroke; patients with ischemic stroke caused by intracranial arterial stenosis (such as stenosis of the intracranial segments of the middle cerebral artery [MCA] and basilar artery [BA]).

Exclusion criteria

The exclusion criteria were head trauma or cerebral hemorrhage detected on CT plain scans; severe motion artifacts caused by patient restlessness; poor image quality due to contrast injection failure, preventing measurement and failing to meet diagnostic requirements; allergy to iodine-based contrast agents; and severe hepatic or renal dysfunction, significant compensated cardiac insufficiency, or pregnancy; patients with intracranial aneurysms, arteriovenous malformations, or other non-stenotic vascular anomalies.

Methods

CTP examinations were performed using a 256-row Revolution Apex CT scanner (GE Healthcare). All patients were positioned supine and given standard breathing instructions during scanning. The scanning range extended from the top of the

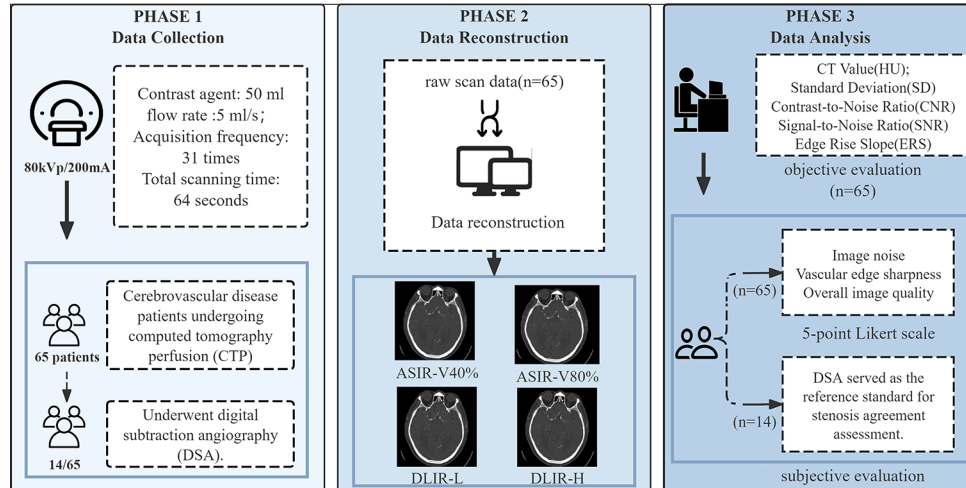


Figure 1: Flowchart of this study. (ASIR-V: adaptive statistical iterative reconstruction-veo; DLIR-L: deep learning low setting; DLIR-H: deep learning high setting).

skull to the skull base, with the direction oriented from head to foot. Scanning began 5 s after contrast agent injection. A total of 31 acquisitions were obtained, specifically (25 acquisitions \times 2 s + 1 acquisition \times 1 s) + (4 acquisitions \times 3 s + 1 acquisition \times 1 s), for a total scanning time of 64 s. The scanning parameters are summarized in Table 1.

Image data processing

The raw CTP data were reconstructed into CTA images at the arterial peak phase using four algorithms: ASIR-V 40% (Group 1), ASIR-V 80% (Group 2), DLIR low setting (DLIR-L) (Group 3), and DLIR high setting (DLIR-H) (Group 4). The reconstructed image datasets for all four groups were transferred to the GE Advanced Workstation 4.7 (AW 4.7) for post-processing.

Objective image quality evaluation

For all four data groups, regions of interest (ROIs) were placed at identical anatomical locations on the M1 segment of the contralateral MCA, BA, internal carotid artery (ICA), and the right temporalis muscle at the level of the hyoid bone. CT attenuation and standard deviation (SD) were then measured. For vascular ROIs, the area selected had to cover more than half of the vascular lumen while avoiding regions affected by calcification, severe stenosis, plaques, or artifacts. The ROI in the temporalis muscle was required to be 1 cm² in area, and the SD of the temporal muscle was selected as background noise. The contrast-to-noise (CNR, Formula 1) and signal-to-noise ratio (SNR, Formula 2) for each group were calculated using the following formulas:

$$CNR = \frac{HU_{Target\ vessel} - HU_{Target\ muscle}}{SD_{Target\ muscle}} \quad (1)$$

$$SNR = \frac{HU_{Target\ vessel}}{SD_{Target\ muscle}} \quad (2)$$

Note: The target muscle refers to the temporalis muscle.

Evaluation of vascular edge sharpness

Edge rise distance (ERD) and edge rise slope (ERS) were used to assess vascular edge sharpness. In the cross-sectional images of all four groups, a straight line was drawn through the center of the BA lumen, extending from the surrounding brain parenchyma. CT attenuation curves were generated using ImageJ software (National Institutes of Health, Bethesda, MD) and its Plot Profile tool for particle analysis. During measurement, calcifications and plaques were carefully avoided. The clone function was applied during curve generation to ensure identical starting and ending positions across the four image groups. The edge response width, defined as the 10–90% ERD, was subsequently measured and calculated. The ERS was calculated using the following formula (3):

$$ERS = \frac{HU_{90\%} - HU_{10\%}}{ERD} \quad [\text{Figure 2}]. \quad (3)$$

Subjective image quality evaluation

Two radiologists with over 5 years of diagnostic imaging experience independently evaluated the original cross-sectional images and post-processed images in a double-blind manner. Image quality was assessed for image noise, vascular edge sharpness, and overall image quality using a 5-point Likert scale, with scores above 3 points considered to meet the diagnostic criteria [Table 2].^[20]

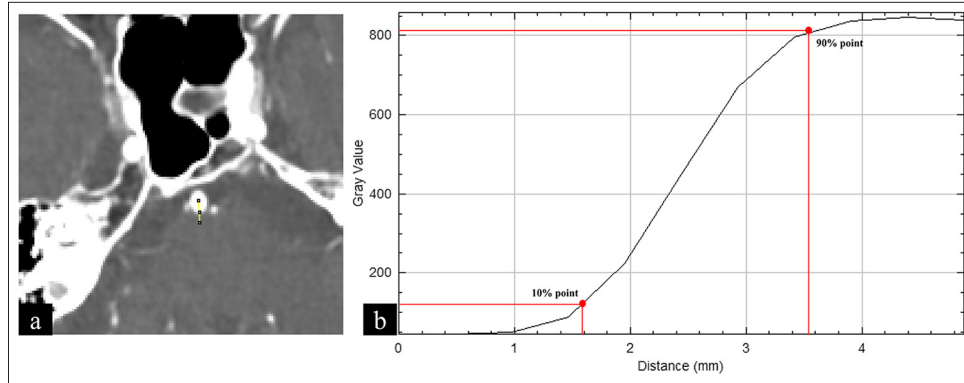


Figure 2: Schematic illustration of edge rise distance (ERD) and edge rise slope (ERS) measurements. (a) A straight line perpendicular to the wall of the basilar artery is drawn. (b) Red dots mark the 10% and 90% points. ERD is defined as the distance between these two points on the computed tomography attenuation curve, while ERS is the slope between them.

Table 1: CT parameters and contrast material protocols.

| Parameters | Value |
|---|-------|
| Scanning parameter | |
| Tube voltage (kV) | 80 |
| Tube current (mA) | 200 |
| Rotation time (s) | 1 |
| Slice thickness (mm) | |
| Scan | 5 |
| Reconstruction | 0.625 |
| Slice interval (mm) | 0.625 |
| Contrast material injection protocol | |
| Iodine concentration (mgI/mL) | 350 |
| Contrast volume (mL) | 50 |
| Contrast injection rate (mL/s) | 5 |
| Saline volume (mL) | 30 |
| Saline injection rate (mL/s) | 5 |

Table 2: Five-point likert scale.

| Score | Image noise | Vascular edge sharpness | Overall image quality |
|-------|---------------------|-------------------------|-----------------------|
| 1 | Unacceptable | Blurry | Unacceptable |
| 2 | Above average | Blurrier than average | Poor |
| 3 | Average | Average | Moderate |
| 4 | Below average | Sharper than average | Good |
| 5 | Minimal or no noise | Sharpest | Excellent |

Evaluation of arterial stenosis degree

With DSA as the reference standard, two radiologists independently analyzed each vascular stenosis or occlusion

lesion identified on DSA images in a double-blind manner and compared these lesions with corresponding images from the four CTA reconstruction datasets. The degree of stenosis was quantified for each affected vessel on both DSA and CTA images. In cases of disagreement, measurements were repeated until consensus was reached. Based on the arterial diameter, the stenosis severity was classified as follows: Mild (1–49%), moderate (50–69%), severe (70–99%), and total occlusion (100%).

Radiation dose

The clinical data collected from each patient included sex, age, computed tomography dose index volume (CTDI_{vol}), and dose length product (DLP). Both CTDI_{vol} and DLP values were automatically generated by the scanner upon completion of the CTP scan. The effective dose (ED) was calculated using the formula $ED = DLP \times k$, where the conversion factor k is 0.0021 mSv/(mGy·cm).^[21]

Statistical analysis

All data were analyzed using the Statistical Package for the Social Sciences for Windows, version 27.0 (IBM Corp., Armonk, NY, USA). Continuous variables are presented as mean±SD. The Kolmogorov–Smirnov test was used to assess normality, and the Levene’s test was used to evaluate variance homogeneity. Categorical data are expressed as frequencies (%). Quantitative data meeting the assumptions of normal distribution and homogeneity of variances are reported as mean±SD. One-way analysis of variance was performed to compare CT attenuation, SD, SNR, and CNR among the four groups, with pairwise comparisons conducted using the least significant difference test. Data not conforming to a normal distribution are expressed as median and interquartile range (M [P25, P75]), with group comparisons performed using the Kruskal–Wallis test and pairwise comparisons using the

Mann–Whitney U test. The intraclass correlation coefficient (ICC) was used to evaluate inter-rater reliability. Agreement between the two radiologists for subjective image quality scores and arterial stenosis grading was assessed using the Kappa statistic. A $p < 0.05$ was considered statistically significant.

RESULTS

Patients' clinical data

| Parameters | Value |
|---------------------|---------------------------|
| Age, years | 68.11±12.76 |
| Sex | 46/19 |
| Male | 46 (70.8%) |
| Female | 19 (29.2%) |
| CTDI _{vol} | 126.13 (108.255, 127.11) |
| DLP | 1779.9 (1692.69, 2018.48) |
| ED | 3.74 (3.55, 4.24) |

Data are presented as mean±standard deviation, n (%), or median (interquartile range). CTDI_{vol}: Computed tomography dose index volume, DLP: Dose length product, ED: Effective dose

A total of 65 patients were included in this study, comprising 46 males (70.8%) and 19 females (29.2%), with a mean age of 68.11 ± 12.76 years. The CTDI_{vol} was 126.13 (108.26, 127.11), the DLP was 1779.90 (1692.69, 2018.48), and the ED was 40.94 (38.93, 46.43) [Table 3].

Objective image quality evaluation

Objective assessment showed no significant differences in CT values among the four image groups ($p > 0.05$). However, SD, CNR, and SNR values for the MCA, ICA, and BA differed significantly among the groups ($p < 0.05$). Both ERD and ERS, which quantify vascular edge sharpness, were significantly better in the DLIR groups than in the ASIR-V groups ($p < 0.05$) [Table 4].

Post hoc comparison of objective image quality evaluation

Pairwise comparisons showed no significant differences in CT values among the four reconstruction algorithms: ASIR-V40%, ASIR-V80%, DLIR-L, and DLIR-H (G1–G4) for any vascular region ($p > 0.05$). In the ICA and BA, SD values in the G4 group were significantly lower than those of the G1 and G2 groups ($p < 0.05$). Regarding both CNR and SNR, no

| Measurement metrics | Group 1 ($n=65$) | Group 2 ($n=65$) | Group 3 ($n=65$) | Group 4 ($n=65$) | p -value |
|---------------------|------------------------|------------------------|-------------------------|-------------------------|------------------|
| MCA | | | | | |
| CT value, HU | 549.24±131.51 | 548.86±131.51 | 570.62±131.83 | 567.04±132.48 | 0.752 |
| SD | 25.2 (19.5, 34.5) | 24.7 (18.2, 34) | 22.7 (17.85, 30.75) | 21.4 (14.65, 28.65) | 0.047 |
| CNR | 29.47 (22.225, 37.27) | 38.98 (28.915, 49.695) | 28.6 (22.06, 41.275) | 39.65 (31.1, 57.67) | <0.001 |
| SNR | 33.17 (24.87, 41.805) | 43.69 (33.43, 57.7) | 32.03 (25.75, 45.985) | 39.65 (31.1, 57.67) | <0.001 |
| ICA | | | | | |
| CT value, HU | 604.5 (532.65, 683.7) | 604.8 (532.55, 684.75) | 615.8 (540.65, 697.35) | 612 (527.5, 681.75) | 0.913 |
| SD | 23.8 (17.95, 28.6) | 21.8 (16.6, 27.1) | 20.1 (15.25, 26.45) | 17 (12.35, 22.35) | <0.001 |
| CNR | 32.46 (25.165, 41.385) | 44 (33.125, 52.93) | 31.63 (24.83, 42.025) | 44.47 (35.025, 60.805) | <0.001 |
| SNR | 37.03 (27.9, 46.8) | 50.86 (37.23, 58.715) | 35.92 (28.415, 48.665) | 44.47 (35.025, 60.805) | <0.001 |
| BA | | | | | |
| CT value, HU | 507.76±127.84 | 506.99±127.08 | 533.55±126.64 | 535.47±125.29 | 0.469 |
| SD | 25.4 (20.45, 30.8) | 25.1 (20.05, 30.15) | 23.2 (17.25, 28.7) | 21.1 (15.3, 25.75) | 0.001 |
| CNR | 24.58 (19.325, 35.685) | 33.16 (25.105, 47.175) | 25.66 (19.65, 39.66) | 35.92 (27.425, 57.475) | <0.001 |
| SNR | 29.71 (22.515, 39.845) | 37.86 (29.115, 54.435) | 29.98 (22.095, 45.2) | 35.92 (27.425, 57.475) | <0.001 |
| Temporalis | | | | | |
| CT value, HU | 68.5 (56.75, 77.1) | 68.2 (56.7, 75.85) | 68.1 (54.3, 74.85) | 66.5 (53.45, 73.15) | 0.889 |
| SD | 16.1 (12.85, 20.55) | 11.9 (10, 16) | 16.6 (12.35, 21.85) | 12.2 (9.3, 14.85) | <0.001 |
| ERD, mm | 1.84±0.36 | 1.79±0.32 | 1.6227 (1.4978, 1.8791) | 1.5857 (1.4934, 1.7957) | 0.001 |
| ERS, HU/mm | 258.08±71.05 | 262.54±69.66 | 293.22±71.65 | 295.42±69.02 | 0.003 |

Data are presented as mean±SD or median (interquartile range). Group 1: ASIR-V 40%, Group 2: ASIR-V 80%, Group 3: DLIR-L, Group 4: DLIR-H. HU: Hounsfield units, SD: Standard deviation, CNR: Contrast-to-noise ratio, CT: Computed tomography, SNR: Signal-to-noise ratio, MCA: Middle cerebral artery, ICA: Internal carotid artery, BA: Basilar artery, Temporalis: Temporalis muscle, ERD: Edge rise distance, ERS: Edge rise slope. Bold type indicates significant differences

Table 5: *Post hoc* comparison of objective image quality evaluation.

| Measurement metrics | G1 versus G2 | G1 versus G3 | G1 versus G4 | G2 versus G3 | G2 versus G4 | G3 versus G4 |
|---------------------|------------------|--------------|------------------|------------------|--------------|------------------|
| MCA | | | | | | |
| CT value | 0.987 | 0.356 | 0.442 | 0.348 | 0.433 | 0.877 |
| SD | 0.554 | 0.264 | 0.008 | 0.573 | 0.029 | 0.094 |
| CNR | <0.001 | 0.579 | <0.001 | 0.004 | 0.265 | <0.001 |
| SNR | <0.001 | 0.773 | 0.005 | 0.002 | 0.427 | 0.016 |
| ICA | | | | | | |
| CT value | 0.980 | 0.503 | 0.657 | 0.482 | 0.652 | 0.760 |
| SD | 0.160 | 0.049 | <0.001 | 0.572 | 0.003 | 0.019 |
| CNR | <0.001 | 0.942 | <0.001 | <0.001 | 0.416 | <0.001 |
| SNR | <0.001 | 0.970 | 0.003 | <0.001 | 0.328 | 0.005 |
| BA | | | | | | |
| CT value | 0.612 | 0.092 | 0.213 | 0.247 | 0.002 | 0.931 |
| SD | 0.612 | 0.153 | 0.001 | 0.349 | 0.005 | 0.048 |
| CNR | <0.001 | 0.524 | <0.001 | 0.007 | 0.131 | <0.001 |
| SNR | <0.001 | 0.539 | 0.003 | 0.003 | 0.684 | 0.017 |
| Temporalis | | | | | | |
| CT value | 0.703 | 0.618 | 0.339 | 0.830 | 0.469 | 0.640 |
| SD | <0.001 | 0.673 | <0.001 | <0.001 | 0.470 | <0.001 |

G1-G4 as defined in the main text. Bold type indicates significant differences. MCA: Middle cerebral artery, CT: Computed tomography, SD: Standard deviation, CNR: Contrast-to-noise ratio, SNR: Signal-to-noise ratio, ICA: Internal carotid artery, BA: Basilar artery, Temporalis: Temporalis muscle

Table 6: Subjective image quality evaluation.

| Variables | G1 | G2 | G3 | G4 | ICC | P-value |
|-------------------------|-----------|------------|-----------|--------------|-------|------------------|
| Image noise | 3.5 (3,4) | 4 (4,4) | 3 (3,3) | 5 (4,5) | 0.884 | <0.001 |
| Vascular edge sharpness | 3.5 (3,4) | 3 (3, 3.5) | 5 (4,5) | 4.5 (4.25,5) | 0.815 | <0.001 |
| Overall image quality | 3.5 (3,4) | 3.5 (3,4) | 3.5 (3,4) | 5 (4.5,5) | 0.797 | <0.001 |

Data are presented as median (interquartile range). ICC: intraclass correlation coefficient, G1, G2, G3, and G4 represent Group 1 (ASIR-V 40%), Group 2 (ASIR-V 80%), Group 3 (DLIR-L), and Group 4 (DLIR-H), respectively. Bold type indicates significant differences

significant difference was observed between the G2 and G4 groups ($p > 0.05$); however, both groups exhibited significantly higher CNR and SNR values than the G1 and G3 groups ($p < 0.05$) [Table 5, Figure 3].

Subjective image quality evaluation

In subjective image quality assessment, Group G4 scored highest for both image noise and overall image quality, with only slightly lower ratings than Group G3 for vascular edge sharpness. The ICC values were 0.884, 0.815, and 0.797, respectively, indicating good inter-observer agreement. In addition, statistically significant differences were observed in the subjective evaluation results across all the aforementioned assessment parameters among the four reconstruction groups ($p < 0.001$) [Table 6].

Post hoc comparison of subjective evaluation indicators

Subjective scoring results showed that G4 had the highest proportion of scores of >4 points for image noise, overall image quality, and vascular edge sharpness [Figure 4]. *Post hoc* comparisons revealed that G4 was significantly superior to G1 and G2 for all three indicators ($p < 0.001$). Compared with G3, G4 also showed significantly higher scores for image noise and overall image quality but no significant difference in vascular edge sharpness ($p = 0.60$) [Table 7].

Evaluation of arterial stenosis degree

DSA identified a total of 26 vascular stenoses: 1 case of mild stenosis, 1 case of moderate stenosis, 5 cases of severe stenosis, and 19 cases of total occlusion. Statistical analysis showed that the DLIR group had the highest agreement with

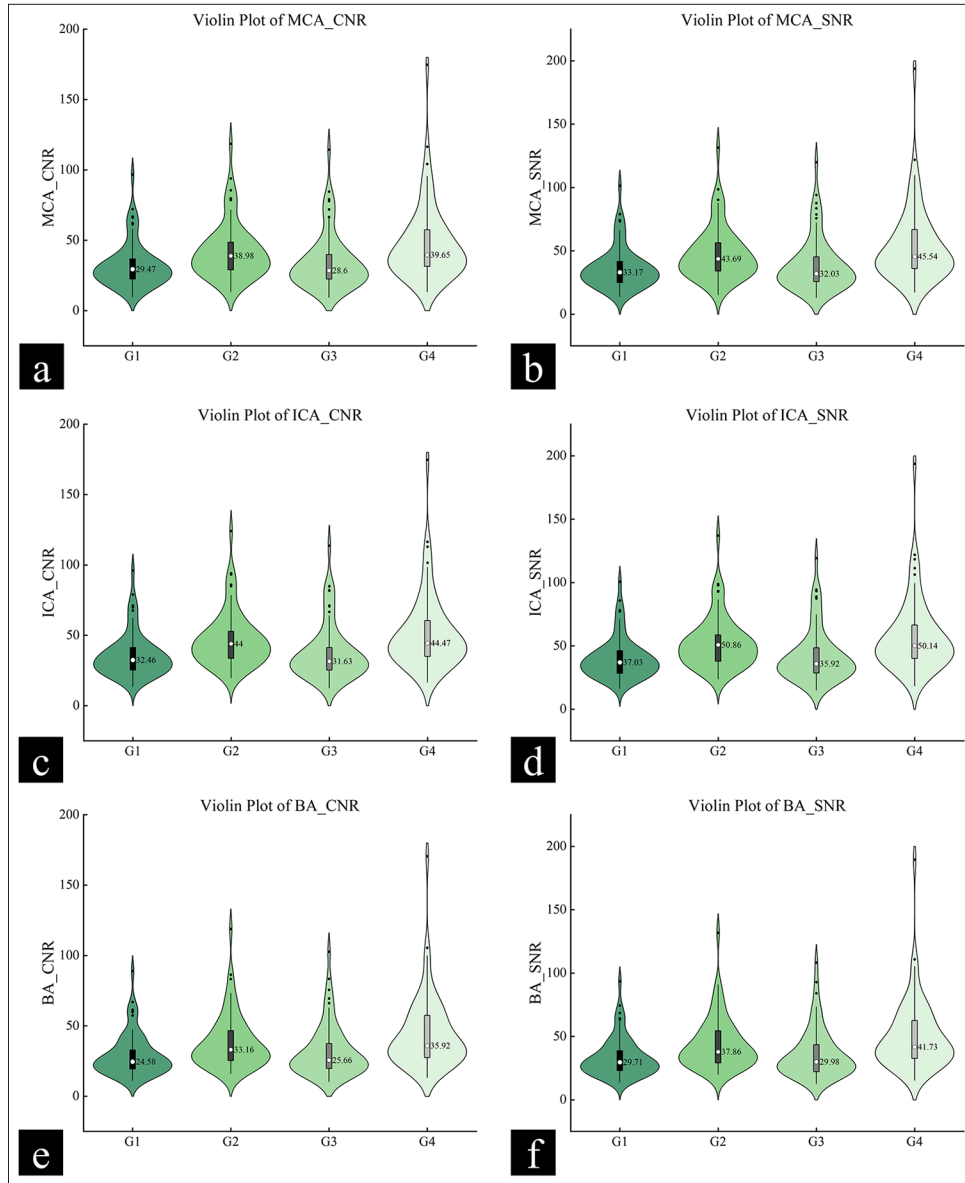


Figure 3: Post hoc comparison of objective image quality evaluation (contrast-to-noise ratio, signal-to-noise ratio). (a) Violin plot of middle cerebral artery (MCA) contrast-to-noise ratio (CNR). (b) Violin plot of MCA signal-to-noise ratio (SNR). (c) Violin plot of internal carotid artery (ICA) CNR. (d) Violin plot of ICA SNR. (e) Violin plot of basilar artery (BA) CNR. (f) Violin plot of BA SNR.

Table 7: Post hoc comparison of subjective evaluation indicators.

| Measurement metrics | G1 versus G2 | G1 versus G3 | G1 versus G4 | G2 versus G3 | G2 versus G4 | G3 versus G4 |
|-------------------------|------------------|------------------|------------------|------------------|------------------|------------------|
| Image noise | <0.001 | <0.001 | <0.001 | <0.001 | <0.001 | <0.001 |
| Vascular edge sharpness | 0.044 | <0.001 | <0.001 | <0.001 | <0.001 | 0.6 |
| Overall image quality | 0.117 | 0.147 | <0.001 | 0.925 | <0.001 | <0.001 |

G1-G4: Corresponding to four distinct image reconstruction schemes described in the main text (specific scheme descriptions align with the main body content). Bold values indicates statistically significant differences (P<0.05) between the compared groups..

DSA ($\kappa = 0.819$, $p < 0.001$), whereas agreement between the ASIR-V group and DSA was only moderate ($\kappa = 0.422$, $p = 0.008$) [Table 8]. Examples of arterial stenosis cases have been shown in Figure 5.

DISCUSSION

In this study, we proposed a more effective reconstruction protocol for cerebral CTA based on CTP data under a low radiation dose. Our results showed that the DLIR-H algorithm was significantly superior to both ASIR-V and DLIR-L in terms of image noise control, CNR, SNR, and diagnostic consistency for vascular stenosis.

Prior studies have compared the performance of ASIR-V and DLIR in different CT applications.^[22,23] In our study, DLIR and ASIR-V were compared specifically for reconstructing cerebral CTA images from 80kVp CTP data. DLIR-H demonstrated markedly better noise suppression than both ASIR-V and DLIR-L at all vascular levels. For example, compared with ASIR-V 40%, DLIR-H reduced the SD by approximately 15.1% (25.2 vs. 21.4), 28.6% (23.8 vs. 17.0), and 16.9% (25.4 vs. 21.1) in the MCA, ICA, and BA. Even against ASIR-V 80%, which has high iterative intensity, DLIR-H still reduced ICA noise by about 22.0% (21.8 vs. 17.0, $p < 0.001$), demonstrating greater noise suppression efficiency. These findings are consistent with those of Jiang *et al.*,^[24] who reported that in ultra-low-dose chest CT for pulmonary nodule detection, DLIR significantly reduced image noise and improved nodule detection rates compared with ASIR-V.

Regarding CNR and SNR, there was no significant difference between the DLIR-H and ASIR-V 80% groups, but both groups were significantly superior to the ASIR-V 40% and DLIR-L groups ($p < 0.001$). This noise reduction pattern may stem from the convergence of the two reconstruction modalities' respective technical advantages and inherent performance ceilings: ASIR-V 80% operates at high iterative intensity, where its noise suppression capacity approaches the upper limit of the statistical iterative framework. Through repeated projection data optimization, it effectively mitigates image noise. In contrast, DLIR-H leverages a deep learning architecture trained on massive imaging datasets to discriminate noise from valid signals; thus, within the specific context of cerebrovascular imaging in the present study, the noise reduction efficacy of these two fundamentally distinct mechanisms achieved a statistically equivalent level of performance. Lei *et al.*^[25] reported in their image quality assessment study that increasing DLIR reconstruction intensity significantly improved both CNR and SNR in white matter and gray matter. This observation highlights the superior utility of DLIR in elevating contrast and signal fidelity for brain tissue imaging. The core conclusion of their work aligns with ours: both studies confirmed that DLIR-H

achieves the highest CNR and SNR, with performance that markedly outperforms low-intensity IR. However, Lei *et al.*^[25] centered their analysis on white matter and gray matter, analyzing the effects of DLIR on brain tissue density differences and perfusion parameters. In contrast, our study targeted cerebrovascular structures (MCA, ICA, and BA). By measuring density differences between vessels and the temporalis muscle to calculate CNR and SNR, we specifically verified the value of DLIR in improving contrast resolution in complex vascular imaging, providing complementary evidence for cerebral CTA vascular assessment based on CTP data.

Previous studies have already confirmed that DLIR-H achieved the highest scores in subjective evaluation of vessels.^[26-27] In our study, DLIR-H achieved the highest ratings for image noise, overall image quality, and vascular edge sharpness and was significantly superior to all other groups. This discrepancy in subjective performance stems from the inherent limitations of statistical IR versus the advantages of deep learning-based frameworks: while ASIR-V80% enhances noise reduction by increasing iterative intensity, its reliance on mathematical model-driven projection data optimization tends to cause excessive smoothing.^[28] This smoothing effect compromises fine anatomical detail preservation and may induce "waxy" artifacts, particularly in complex vascular regions.^[18,25,28] In contrast, DLIR-H is built on convolutional neural networks trained on large-scale high-dose imaging datasets, enabling it to selectively suppress noise while retaining native image texture and vascular edge details.^[29] This unique advantage allows DLIR-H to outperform ASIR-V80% in subjective quality, addressing the trade-off between noise reduction and detail. Our findings demonstrate that DLIR-H effectively mitigates high image noise associated with low-dose 80 kVp scanning, which arises from insufficient photon flux,^[30-31] while facilitating the precise visualization of vascular anatomical details and ensuring patient radiation safety. To further validate the subjective evaluation of vascular edge sharpness, we measured ERD and ERS of the BA as objective indicators. Both ERD and ERS were significantly better in the DLIR groups than in the ASIR-V groups ($P < 0.05$), with DLIR-H performing best overall, owing to DLIR-H images exhibiting significantly increased CT attenuation at vascular-tissue interfaces, which contributed to substantially higher ERS values. These findings confirm that DLIR-H can improve vascular edge sharpness in cerebral CTA reconstructed from CTP data.

In addition, unlike previous studies on brain CTA reconstructed from CTP, this study used DSA as a reference to compare the accuracy of four reconstruction techniques in diagnosing arterial stenosis on CTA. Our results showed that DLIR demonstrated significantly higher agreement with DSA in stenosis assessment ($\kappa = 0.819$, $p < 0.001$)

Table 8: Evaluation of arterial stenosis degree.

| DSA (n=26) | ASIR-V 40% (n=26) | | | | ASIR-V 80% (n=26) | | | | DLIR-L (n=26) | | | | DLIR-H (n=26) | | | |
|------------|-------------------|-----|-----|------|-------------------|-----|-----|------|---------------|-----|-----|------|---------------|-----|-----|------|
| | M | Mod | Sev | Occl | M | Mod | Sev | Occl | M | Mod | Ser | Occl | M | Mod | Sev | Occl |
| M | 1 | 0 | 0 | 0 | 1 | 0 | 0 | 0 | 1 | 0 | 0 | 0 | 1 | 0 | 0 | 0 |
| Mod | 0 | 0 | 1 | 0 | 0 | 0 | 1 | 0 | 0 | 1 | 0 | 0 | 0 | 1 | 0 | 0 |
| Sev | 0 | 0 | 2 | 3 | 0 | 0 | 2 | 3 | 0 | 0 | 4 | 1 | 0 | 0 | 4 | 1 |
| Occl | 0 | 0 | 2 | 17 | 0 | 0 | 2 | 17 | 0 | 0 | 1 | 18 | 0 | 0 | 1 | 18 |
| P-value | 0.008 | | | | 0.008 | | | | <0.001 | | | | <0.001 | | | |
| K-value | 0.422 | | | | 0.422 | | | | 0.819 | | | | 0.819 | | | |

M: Mild stenosis, Mod: Moderate stenosis, Sev: Severe stenosis, Occl: Total occlusion, DSA: Digital subtraction angiography, ASIR-V: Adaptive statistical iterative reconstruction-Veo, DLIR: Deep learning image reconstruction. Vessels that appeared normal on the gold standard DSA images were not included in the comparative evaluation. Bold type indicates significant differences. Bold values: Bold values indicates statistically significant differences (P<0.05) between the compared groups.

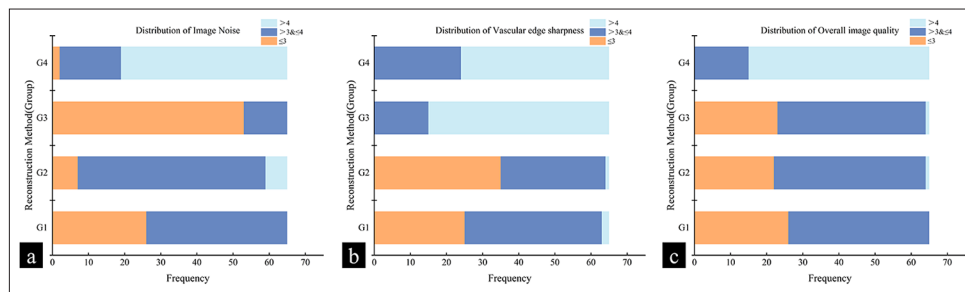


Figure 4: Stacked bar chart of subjective image quality scores (5 points = excellent). (a) Distribution of image noise. (b) Distribution of vascular edge sharpness. (c) Distribution of overall image quality. Light blue: >4 (Excellent); Blue: >3 & ≤4 (Good); Orange: ≤3 (Average).

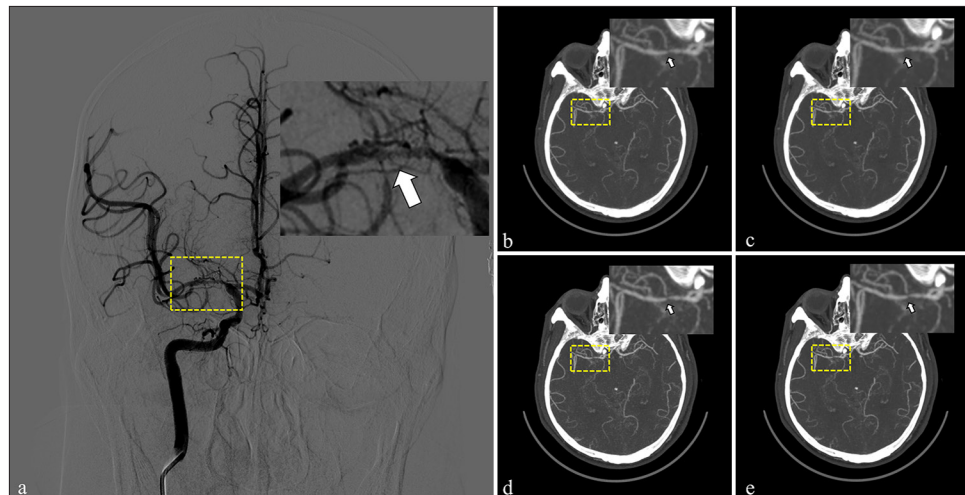


Figure 5: Severe stenosis of the M1 segment of the right middle cerebral artery (MCA) on digital subtraction angiography (DSA) and computed tomography angiography (CTA) reconstructions using different algorithms. A 57-year-old male underwent both computed tomography perfusion and DSA examinations. (a) The DSA image shows severe stenosis in the M1 segment of the right MCA (white arrow). Reconstructed axial MIP images from the CTA using (b) adaptive statistical iterative reconstruction-veo (ASIR-V) 40%, (c) ASIR-V 80%, (d) deep learning image reconstruction (DLIR)-L, and (e) DLIR-H also demonstrate severe stenosis in the same segment (white arrow). Figure (a), DSA image: yellow box = stenotic right MCA M1 segment; Figures (b) to (e), CTA reconstruction images: yellow box = corresponding DSA stenotic segment. The yellow boxes in (b)–(e) indicate the corresponding DSA stenotic segment on the CTA reconstructions.

compared with ASIR-V ($\kappa = 0.422$, $p = 0.008$). This finding is consistent with Qu *et al.*,^[32] who reported that the DLIR's diagnostic accuracy in lower extremity CTA approaches that of DSA. Previous studies have revealed that DLIR optimizes reconstruction through a deep learning model, markedly improving vascular boundary clarity while suppressing noise. Qu *et al.*^[32] showed that in low-dose lower extremity CTA, the ERS of DLIR-H was significantly higher than that of ASIR-V, indicating clearer depiction of vascular wall details. Wang *et al.*^[33] demonstrated in coronary CTA that DLIR-H provides higher spatial resolution for visualizing calcified plaques and intra-stent lumens, offering key morphological evidence for stenosis diagnosis. Compared to ASIR-V, the model characteristics of DLIR make it more suitable for evaluating vascular details under low-contrast conditions. In a phantom-based study, Euler *et al.*^[34] found that for low-contrast tissues, especially at low radiation doses, the spatial resolution of ASIR-V was inferior to that of FBP, with the effect worsening at higher ASIR-V blending levels. By contrast, DLIR-H facilitates the optimization of image noise distribution: It significantly suppresses image noise while enhancing spatial resolution and preserving native image texture, ultimately resulting in clearer vascular boundaries.^[35] These advantages likely explain the higher consistency of DLIR with DSA in stenosis diagnosis observed under the specific conditions of 80 kVp, low radiation, and low contrast in our study.

However, this study has several limitations. First, as a single-center retrospective study with a relatively small sample size, its findings require further validation through larger, multicenter datasets. Second, the range of reconstruction intensities compared was limited. Only ASIR-V 40%, ASIR-V 80%, and DLIR were included; other iterative intensity levels were not assessed, making it difficult to fully characterize the impact of different reconstruction parameters on image quality. Finally, the use of the gold standard was limited because relatively few patients underwent concurrent DSA examinations, which may reduce the strength of our verification of CTA-based stenosis diagnosis.

CONCLUSION

The DLIR-H algorithm significantly improves the image quality of cerebral CTA reconstructed from CTP data by effectively reducing noise, enhancing CNR and SNR, and optimizing diagnostic performance. It can therefore be recommended as the preferred clinical reconstruction approach.

Ethical approval: The research/study was approved by the Institutional Review Board at the Medical Ethics Committee of the Affiliated Hospital of Xuzhou Medical University, number XYFY2025-KL283-01, dated 09 July, 2025.

Declaration of patient consent: Patient's consent is not required as patients identity is not disclosed or compromised.

Financial support and sponsorship: The project "IVC - type B - CS integrated hemodynamic parameter and numerical simulation technology and clinical research" (Grant No. KCJ8209), the Special Fund for Overseas Training of Employees of the Affiliated Hospital of Xuzhou Medical University, which enabled the completion of this study, and the Affiliated Hospital of Xuzhou Medical University Institutional Research Project (2024ZY08).

Conflicts of interest: There are no conflicts of interest.

Use of artificial intelligence (AI)-assisted technology for manuscript preparation: The authors confirm that there was no use of artificial intelligence (AI)-assisted technology for assisting in the writing or editing of the manuscript and no images were manipulated using AI.

REFERENCES

1. Zhou L, Song X, Wang J, Tan Y, Yang Q. Effects of vitamin B12 deficiency on risk and outcome of ischemic stroke. *Clinical Biochem* 2023;118:110591.
2. GBD 2019 Stroke Collaborators. Global, regional, and national burden of stroke and its risk factors, 1990-2019: A systematic analysis for the global burden of disease study 2019. *Lancet Neurol* 2021;20:795-820.
3. Santana Baskar P, Cordato D, Wardman D, Bhaskar S. In-hospital acute stroke workflow in acute stroke - systems-based approaches. *Acta Neurol Scand* 2021;143:111-20.
4. Zhang J, Xie Q, Mou L, Zhang D, Chen D, Shan C, *et al.* DSCA: A digital subtraction angiography sequence dataset and spatio-temporal model for cerebral artery segmentation. *IEEE Trans Med Imaging* 2025;44:2515-27.
5. Seiler A, Lauer A, Deichmann R, Nöth U, Herrmann E, Berkefeld J, *et al.* Signal variance-based collateral index in DSC perfusion: A novel method to assess leptomeningeal collateralization in acute ischaemic stroke. *J Cereb Blood Flow Metab* 2020;40:574-87.
6. Campbell BC, De Silva DA, Macleod MR, Coutts SB, Schwamm LH, Davis SM, *et al.* Ischaemic stroke. *Nat Rev Dis Primers* 2019;5:70.
7. Zeng D, Zeng C, Zeng Z, Li S, Deng Z, Chen S, *et al.* Basis and current state of computed tomography perfusion imaging: A review. *Phys Med Biol* 2022;67:8717.
8. Yang L, Zhang H, Sheng J, Wang M, Liu Y, Xu M, *et al.* Contrast enhancement boost improves the image quality of CT angiography derived from 80-kVp cerebral CT perfusion data. *BMC Med Imaging* 2024;24:193.
9. Kortman HG, Smit EJ, Oei MT, Manniesing R, Prokop M, Meijer FJ. 4D-CTA in neurovascular disease: A review. *AJNR Am J Neuroradiol* 2015;36:1026-33.
10. Lu SS, Zhang X, Xu XQ, Cao YZ, Zhao LB, Liu QH, *et al.* Comparison of CT angiography collaterals for predicting target perfusion profile and clinical outcome in patients with acute ischemic stroke. *Eur Radiol* 2019;29:4922-9.
11. Li K, Garrett J, Ge Y, Chen GH. Statistical model based iterative reconstruction (MBIR) in clinical CT systems. Part II. Experimental assessment of spatial resolution performance. *Med Phys* 2014;41:071911.

12. Park HJ, Choi SY, Lee JE, Lim S, Lee MH, Yi BH, *et al.* Deep learning image reconstruction algorithm for abdominal multidetector CT at different tube voltages: Assessment of image quality and radiation dose in a phantom study. *Eur Radiol* 2022;32:3974-84.
13. Ren Z, Zhang X, Hu Z, Li D, Liu Z, Wei D, *et al.* Reducing radiation dose and improving image quality in CT portal venography using 80 kV and adaptive statistical iterative reconstruction-V in slender patients. *Acad Radiol* 2020;27:233-43.
14. Jiang C, Jin D, Liu Z, Zhang Y, Ni M, Yuan H. Deep learning image reconstruction algorithm for carotid dual-energy computed tomography angiography: Evaluation of image quality and diagnostic performance. *Insights Imaging* 2022;13:182.
15. Sarker IH. Deep learning: A comprehensive overview on techniques taxonomy applications and research directions. *SN Comput Sci* 2021;2:420.
16. Peppert F, Von Kleist M, Schutte C, Sunkara V. On the sufficient condition for solving the gap-filling problem using deep convolutional neural networks. *IEEE Trans Neural Netw Learn Syst* 2022;33:6194-205.
17. Sun J, Li H, Gao J, Li J, Li M, Zhou Z, *et al.* Performance evaluation of a deep learning image reconstruction (DLIR) algorithm in “double low” chest CTA in children: A feasibility study. *Radiol Med* 2021;126:1181-8.
18. Zhong J, Wang L, Shen H, Li J, Lu W, Shi X, *et al.* Improving lesion conspicuity in abdominal dual-energy CT with deep learning image reconstruction: A prospective study with five readers. *Eur Radiol* 2023;33:5331-43.
19. Caruso D, De Santis D, Del Gaudio A, Guido G, Zerunian M, Polici M, *et al.* Low-dose liver CT: Image quality and diagnostic accuracy of deep learning image reconstruction algorithm. *Eur Radiol* 2024;34:2384-93.
20. Abdellatif W, Esslinger E, Kobes K, Wong A, Powell J, Ali IT, *et al.* Acquisition time, radiation dose, subjective and objective image quality of dual-source CT scanners in acute pulmonary embolism: A comparative study. *Eur Radiol* 2020;30:2712-21.
21. Christner JA, Kofler JM, McCollough CH. Estimating effective dose for CT using dose-length product compared with using organ doses: Consequences of adopting international commission on radiological protection publication 103 or dual-energy scanning. *AJR Am J Roentgenol* 2010;194:881-9.
22. Li Y, Liu X, Zhuang XH, Wang MJ, Song XF. Assessment of low-dose paranasal sinus CT imaging using a new deep learning image reconstruction technique in children compared to adaptive statistical iterative reconstruction V (ASiR-V). *BMC Med Imaging* 2022;22:106.
23. Kim I, Kang H, Yoon HJ, Chung BM, Shin NY. Deep learning-based image reconstruction for brain CT: Improved image quality compared with adaptive statistical iterative reconstruction-Ve0 (ASiR-V). *Neuroradiology* 2021;63:905-12.
24. Jiang B, Li N, Shi X, Zhang S, Li J, De Bock GH, *et al.* Deep learning reconstruction shows better lung nodule detection for ultra-low-dose chest CT. *Radiology* 2022;303:202-12.
25. Lei L, Zhou Y, Guo X, Wang L, Zhao X, Wang H, *et al.* The value of a deep learning image reconstruction algorithm in whole-brain computed tomography perfusion in patients with acute ischemic stroke. *Quant Imaging Med Surg* 2023;13:8173-89.
26. Tang Y, Zhang H, Chen L, Yu M, Zhang H, Zhang D, *et al.* Comparison of image quality of 40 keV virtual monoenergetic images of vertebral arteries using DLIR and ASiR-V algorithms under a dual-low scanning protocol. *Eur J Radiol* 2025;191:112276.
27. Zhang Q, Lin Y, Zhang H, Ding J, Pan J, Zhang S. The application value of a vendor-specific deep learning image reconstruction algorithm in “triple low” head and neck computed tomography angiography. *Quant Imaging Med Surg* 2024;14:2955-67.
28. Kwon H, Cho J, Oh J, Kim D, Cho J, Kim S, *et al.* The adaptive statistical iterative reconstruction-V technique for radiation dose reduction in abdominal CT: Comparison with the adaptive statistical iterative reconstruction technique. *Br J Radiol* 2015;88:20150463.
29. Liu M, Chen X, Liu W, Guo Y, Zhu Y, Duan Y, *et al.* Effect of deep learning image reconstruction with high-definition standard scan mode on image quality of coronary stents and arteries. *Quant Imaging Med Surg* 2024;14:1616-35.
30. Wu X, Yang Y, Wen M, Wang L, Yang Y, Zhang Y, *et al.* Ultra-low-dose multiphase CT angiography derived from CT perfusion data in patients with middle cerebral artery stenosis. *Neuroradiology* 2020;62:167-74.
31. Wang T, Gong Y, Shi Y, Hua R, Zhang Q. Feasibility of dual-low scheme combined with iterative reconstruction technique in acute cerebral infarction volume CT whole brain perfusion imaging. *Exp Ther Med* 2017;14:163-8.
32. Qu T, Guo Y, Li J, Cao L, Li Y, Chen L, *et al.* Iterative reconstruction vs deep learning image reconstruction: Comparison of image quality and diagnostic accuracy of arterial stenosis in low-dose lower extremity CT angiography. *Br J Radiol* 2022;95:20220196.
33. Wang Y, Wang G, Huang X, Zhao W, Zeng Q, Li Y, *et al.* Improving image quality and resolution of coronary arteries in coronary computed tomography angiography by using high-definition scans and deep learning image reconstruction. *Quant Imaging Med Surg* 2023;13:2933-40.
34. Euler A, Solomon J, Marin D, Nelson RC, Samei E. A third-generation adaptive statistical iterative reconstruction technique: Phantom study of image noise, spatial resolution, lesion detectability, and dose reduction potential. *AJR Am J Roentgenol* 2018;210:1301-8.
35. Racine D, Becce F, Viry A, Monnin P, Thomsen B, Verdun FR, *et al.* Task-based characterization of a deep learning image reconstruction and comparison with filtered back-projection and a partial model-based iterative reconstruction in abdominal CT: A phantom study. *Phys Med* 2020;76:28-37.

How to cite this article: Zhang L, Feng X, Zhang H, Zhang D, Zhao H, Sun Q, *et al.* Optimization of image quality and diagnostic accuracy for vascular stenosis in computed tomography perfusion-reconstructed cerebral computed tomography angiography using deep learning reconstruction. *J Clin Imaging Sci.* 2026;16:12. doi: 10.25259/JCIS_226_2025